Bordbar, Hadi; Hostikka, Simo; Boulet, Pascal; Parent, Gilles

Numerically resolved line by line radiation spectrum of large kerosene pool fires

Published in:
Journal of Quantitative Spectroscopy and Radiative Transfer

DOI:
10.1016/j.jqsrt.2020.107229

Published: 01/10/2020

Document Version
Peer-reviewed accepted author manuscript, also known as Final accepted manuscript or Post-print

Numerically Resolved Line by Line Radiation Spectrum of Large Kerosene Pool Fires[1]

Hadi Bordbar[*1], Simo Hostikka[1], Pascal Boulet[2], Gilles Parent[2]
[1]Department of Civil Engineering, Aalto University, Finland.
[2]Université de Lorraine, CNRS, LEMTA, F-54000 Nancy, France.
[*]Corresponding author: Hadi Bordbar (hadi.bordbar@aalto.fi)

ABSTRACT

A numerical model is presented for spectral characteristics of radiation coming from a pool fire flame. The case studies are 1.75m ×1.75m and 2.5m×2.5m Kerosene pool fires. Transient heat and mass transfer of the system was solved using a CFD model of a 4m×4m×5m rectangular domain built in Fire Dynamic Simulator (FDS) with LES of turbulence and a two-step combustion reaction. Transient profiles of gas compositions, soot concentration and temperature along a line of sight of an imaginary sensor were collected from the CFD simulations, and instantaneous solutions of the thermal radiation along the line were calculated using high-resolution LBL spectral absorption profiles of combustion gases together with a model for soot absorption coefficient, based on spectrally dependent complex index of refraction. The transient spectra, consisting of numerous instantaneous intensity solutions, were then averaged and compared against the similar experimentally measured data. The line of sight and other settings of the model were carefully checked to be consistent with the experiments performed for the same system. The modelling results revealed the strong absorption effect of cold atmospheric gases while the emission peak of hot CO_2 at ~2200 cm^{-1} in fire is still quite distinguishable from the spectral profile of hot blackbody even at 23 m away from the center of the flame. This emission peak can be therefore used for detection of the fire. The spectral changes of the spectrum are explained and a sensitivity analysis is performed to study the effects of the sensor's distance from the pool, pool size, and modeling and operational conditions, such as relative humidity and radiative fraction.

INTRODUCTION

1 The article can be cited as: Bordbar H., Hostikka S., Parent G., Boulet P., (2020) "Numerically Resolved Line by Line Radiation Spectrum of Large Kerosene Pool Fires", *Journal of Quantitative Spectroscopy and Radiative Transfer,* Vol. 254, pp.107229 https://doi.org/10.1016/j.jqsrt.2020.107229.

With the recent improvement in available computational resources, the role and capabilities of numerical modeling in design and analysis of energy conversion systems is more and more highlighted [1]. The available computational resource among the improvement in numerical methods paved the road to analyze many of complex physical phenomena involved in analysis of energy conversion systems such as combustion [2], multiphase flows [3, 4, 5], and thermal radiation [6, 7]. Thermal radiation plays an important role in heat transfer, spreading, and expansion of fires [8, 9]. The spectral characteristics of fire flames are important in several ways. In pool fires, radiation reaching the liquid surface is the main source of heating and evaporation, and therefore controls the pool's heat release rate [8]. Moreover, spectral characteristics of fires can be used to detect the fires, distinguishing it from the spectral radiation from a hot object or solar radiation [10].

Within the part of electromagnetic wave spectrum where the radiation heat transfer occurs, the gas spectral absorption coefficient profile forms a histogram containing millions of absorption lines. Much attention has been devoted in the last decades to develop numerical models that could feasibly take the variation of the spectral absorption coefficients of the gases into account [11]. The most well-known simplifying methods such as weighted sum of gray gases model (WSGG) [12] or full spectrum correlated-k method (FSCKM) [13, 7] aim at providing accurate total heat flux and heat source but they do not provide any information about spectral variation of radiation intensity. While the box models can provide spectral flux, they need large number of bands to reach to a satisfactory level of accuracy [14]. Moreover, their results depend a lot on selection of band limits which are usually not theoretically sound [15].

The most accurate prediction of the spectral radiative properties is obtained by the so-called line by line calculation (LBL) that implements spectroscopic databases containing a set of spectral line parameters required to calculate the spectral absorption coefficient for the specified spectral location. Due to the high computational cost of LBL, its usage is limited to providing the data needed for development of other methods [16] or obtaining benchmark solutions for their validation. While LBL data have been widely used to obtain benchmark reference solution in one-dimensional slab problem, i.e. a medium with a known temperature and gas composition profiles bounded between two infinitely large parallel plates problems [17, 14, 12], Fraga et al. [18] has recently developed a benchmark solution for a few artificial three-dimensional air and oxygen fired flames by using the high resolution LBL absorption spectra of CO_2 and H_2O in solving Radiative Transfer Equation (RTE) with a discrete ordinate method implementing very fine spatial and directional discretization.

In the current study, however, we use high-resolution LBL absorption spectra of H_2O, CO_2 and CO to obtain the spectral intensity going out of flame zone of a large pool fire. The researches aimed at identifying the characteristics of thermal radiation spectra of fires are quite rare. Due to experimental challenges, spectrally resolved measurements of the radiation emitted by a flame are not so common,

and spectral calculations are even less common, especially with high-resolution. In one of the few experimental attempts, Suo-Antilla et al. [19] experimentally measured the thermal radiation spectrum of a 2m pool fires reaching the pool surface using a mid-infrared spectrometer. They could identify the contributions of soot and gases in overall emission of the flame for four different fuels including n-heptane. They noticed the large absorption effect of a fuel rich region close to the pool surface compared to the absorption from within the flame zone [19]. Parent et al. [20] recently measured the thermal radiation spectra at 23 m distance from 0.7-2.5 m Kerosene pool flames. Using an opacimeter setup together with a FTIR spectrometer, they reported the emittance values and equivalent soot temperatures. The atmospheric cold gases caused the major absorption bands in their measured spectra while a peak at ~ 2200 cm^{-1} was clearly seen in their results which is guessed to be because of emission of hot CO2 inside the flame zone.

While experimental work in this field is quite a few, the present paper beside our previous report in ICHMT-Rad19 symposium [21] is to the best of our knowledge the first numerical work which provides a validated numerical methodology to calculate the high resolution flame spectra of large pool fires. Here in this study we present a novel numerical approach to predict the thermal radiation spectra outside pool fires. The hydrodynamics and reaction of a pool fire was solved by Fire Dynamics Simulator (FDS). FDS is a computational fluid dynamics (CFD) code for simulating the fire-driven fluid flow [22]. Extracting the transient data along a line of sight of a sensor from the CFD model, a separate one-dimensional model was then built up to solve spectral radiation and provide the line by line intensity spectrum reach a point out of the flame zone. A mesh independency analysis was done for the CFD model. The line-by-line absorption spectra of combustion gases were obtained using the HITEMP2010 database [23]. The one-dimensional model is based on solving a line of sight which is passing through the flame and reach a sensor as in the experimental setup.

The case studies are two square shaped Kerosene pool fires of 1.75m×1.75m and 2.5m×2.5m. The resolution of numerically obtained radiation spectra is 0.02cm^{-1} which is much higher than that of experimental data, i.e. 4 cm^{-1}. The experimental spectra were acquired with a Fourier Transform Infrared (FTIR) spectrometer in the spectral range 800 cm^{-1} – 6000 cm^{-1}. The unique spectral features of the fire spectra are discussed and the effect of hot emitting gases within the flame zone and cold atmospheric absorbing gases outside the flame zone are addressed. A sensitivity analysis will be presented to address effect of the pool size, sensor's distance from the pool, radiative fraction used in FDS calculations and relative humidity of the air.

EXPERIMENTAL SETUP

Experiments were conducted in a former aircraft hangar made available by Aéroport de Paris (Orly, France). This building allowed large size pool fires. Its dimensions are large enough to consider that fire occurred in open space while being protected from rain and wind. Square pans of dimensions 250 × 250 cm, 175 × 175 cm, 100 × 100 cm and 70 × 70 cm were used from which the results of the first two are used in this research for validation of numerical data. Pan height was 20 cm, and was made with welded 4 mm thick steel sheets. A 5 cm high layer of Jet-A1 kerosene was laid onto a 10 cm layer of water used to stabilize the kerosene mass loss rate (MLR). The liquid level was not kept constant, and tests were conducted until flame out. Kerosene mass was measured thanks to a scale, except for the largest pool due to its too large weight. The MLR was roughly constant during a 10 to 20 minutes steady phase. Radiation emitted by the flame was recorded with a FTIR spectrometer, Bruker® Matrix®, along a horizontal line of sight, 20 cm above the pan. Spectral resolution was 4 cm^{-1} and useful spectral range was 800 cm^{-1} – 6000 cm^{-1}. The distance between the center of the pan and the spectrometer was 23 m. The spectrometer was calibrated with a cavity blackbody (Mikron® model M330EU) at 1200°C allowing to obtain the radiative intensity expressed in $W/(m^2.sr.cm^{-1})$ received by the spectrometer. Required acquisition time for a spectrum at full resolution was around 0.2 s. FTIR spectra are the Fourier transform of the interferograms acquired by the spectrometer and low resolution information of a spectrum is contained in a very small time interval around the so-called center-burst of the interferogram. Thus spectra can be considered almost instantaneous. Depending on the test duration, 70 to 95 spectra were averaged over the steady phase of the fire during which the MLR was almost constant. More details of the experimental setup can be found in [20, 24].

NUMERICAL METHODOLOGY

3D CFD model

A three-dimensional CFD model was built to solve heat and mass transfer of 1.75m and 2.5m square Kerosene pool fires using Fire Dynamics Simulator (FDS) as shown in Figure 1. The geometry of the model was a 4m×4m×5m box in which all the walls, except the bottom one, were considered open. It made the model consistent with the experiments. Two computational grids with uniform Cartesian mesh with a characteristic length of 5cm and 1cm, have been used to solve the hydrodynamics, turbulence, combustion and heat transfer. The FDS model employs a number of simplifications of the governing equations that allow for relatively fast simulations of practical fire scenarios [22]. The low-Mach number hydrodynamic model consists of large-eddy simulation sub-grid closure with Deardorff model for turbulent viscosity. Combustion is typically treated as a mixing controlled, single-step reaction of fuel and oxygen [22]. However, for the present modelling work, we used a two-step simple reaction model of FDS [25]. The two-step scheme basically takes all of the

carbon in the fuel molecule and converts it to CO and soot in the first step, and then oxidizes most of the CO and soot to form CO_2 in the second step [25]. The hydrogen in the fuel molecule can form either H_2 or H_2O in the first step as well [25]. In the setting of the present work, two-thirds of the carbon atoms in the fuel are converted to CO. There is not yet a solid basis for this assumption, and the conversion ratio of carbon to CO and soot can be tuned. The radiation transport equation is written in terms of a spectrally-averaged grey gas [22]. FDS uses the narrow band code of RADCAL [26] to calculate an effective gray absorption coefficient for gas-soot mixture. The participating species in our model are CO_2, H_2O, n-dodecane and CO in addition to soot. The RADCAL surrogates n-dodecane with n-heptane in its calculations.

The default model of RADCAL for calculating soot spectral absorption coefficient is replaced by a model accounting for spectral variation of refractive index of soot according to Rayleigh theory. The spectral absorption coefficient of soot cloud (κ_s) is calculated as:

$$\kappa_s = \alpha_\eta \nu_s \eta \tag{1}$$

where ν_s and η represent the soot volume fraction and wavenumber, respectively. The parameter α_η has been assumed constant in many researches leading to a linear relation between the soot spectral absorption coefficient and wavenumber. However, the experimental observations do not prove the perfect linear relation [27, 28]. The experimental measurements done by Chang and Charalampopoulos [27] proposed two correlations for the real (n_s) and imaginary (k_s) parts of the complex index of refraction of soot which account for their dependency to wavelength (or wavenumber) as:

$$n_s = 1.811 + 0.1263ln(\lambda) + 0.027ln^2(\lambda) + 0.0417ln^3(\lambda) \tag{2}$$

$$k_s = 0.5821 + 0.1213ln(\lambda) + 0.2309ln^2(\lambda) - 0.01ln^3(\lambda) \tag{3}$$

where $\lambda[\mu m]$ represents wavelength and is given as $\lambda[\mu m] = \frac{10000}{\eta[cm^{-1}]}$. Using the spectral complex index of refraction of soot particles, one can obtain the α_η values assuming Rayleigh regime for a cloud of soot particles as [27, 28]:

$$\alpha_\eta = \frac{36\pi n_s k_s}{(n_s^2 - k_s^2 + 2)^2 + 4\pi n_s^2 k_s^2} \tag{4}$$

Substituting the calculated α_η in Eq.1, the spectral absorption coefficient of soot was obtained and used in the CFD and 1D-LBL calculation of the present work.

The finite volume method [29] is used to solve the thermal radiation in FDS using 104 discrete angles which are updated over 15 time steps [22].

Due to the coarse computational grid used in typical fire simulations, the computed temperature of a grid cell represents a bulk average over the cell volume. In the region where combustion occurs, the computed temperature may be considerably lower than the true flame sheet temperature in a diffusion flame [22]. It is also partly due to skipping the turbulence-radiation interaction in sub-grid scales. As the radiation source term is proportional to T^4, the temperature underpredictions propagate and magnify in the radiation source term. These errors are assumed to be significant within a "flaming region" that consists of the cells where the local, nominal radiative loss $\chi_r q''' > 10\ \mathrm{kW/m^3}$, in which χ_r is the fraction of the total combustion energy q''' that is locally released in the form of thermal radiation [30]. Outside the flaming region, the average cell temperature yields an accurate value of radiative emission and can be used directly in the solution of the RTE. Within the flaming region, the emission term of the RTE is corrected using a factor C [30]:

$$I_{b,f}(x) = C\frac{\sigma T(x)^4}{\pi} \text{ where } C = \min\left[100, \max\left(1, \frac{\sum_{q'''_{ijk}>0}\left(\chi_r q'''_{ijk} + \kappa_{ijk} I_{ijk}\right)dV}{\sum_{q'''_{ijk}>0}\left(4\kappa_{ijk}\sigma T_{ijk}^4\right)dV}\right)\right] \quad (5)$$

Here $T, \kappa_{ijk}, I_{ijk}, \chi_r, V$ and σ are temperature [K], absorption coefficient, directionally integrated intensity, radiative fraction, volume and Stefan-Boltzmann constant, respectively. Using this correction factor, the net radiative emission from the flaming region approaches the desired (global) fraction of the total heat release rate. For most of the fuels, the radiative fraction (χ_r) have been reported between 0.3-0.4. For this size of Kerosene pool fire, radiative fraction of 0.3 has been reported [31] and is used in this work. To study the sensitivity of the results to the radiative fraction modelling, the simulations are also performed with $\chi_r = 0$, in which case no correction is introduced to the emission term, i.e. $C = 1$ in Eq. 5. Nonetheless, even for this case, the share of radiation of the overall global heat release rate (which is equivalent to radiative fraction) will be predicted through Eq. 5 and can be extracted from the FDS results.

The pool is modelled as a fuel mass inflow boundary with corresponding to a heat release rate of 1683.121 kW/m^2, calculated by an empirical correlation [32]:

$$HRRPUA = \dot{m}\Delta h = \dot{m}_\infty(1 - e^{-k\beta D})\Delta h \quad (6)$$

where D and Δh represent diameter of the pool and enthalpy of combustion. Due to similar thermodynamic properties [33], n-Dodecane is used as the surrogate of Kerosene. The parameter $k\beta$

and $\dot{m}_{\infty}$are given as 3.5 m^{-1}, and 0.039 kg/m^2s for Kerosene liquid pool fire [22]. All the domain boundaries except the pool surface and bottom boundary are considered open. The setting of the pool in the fire is representing the MLR of the steady state period of the experiments and therefore, the results of the modeling is consistent with the measurements which were done for steady state period of the pool fires.

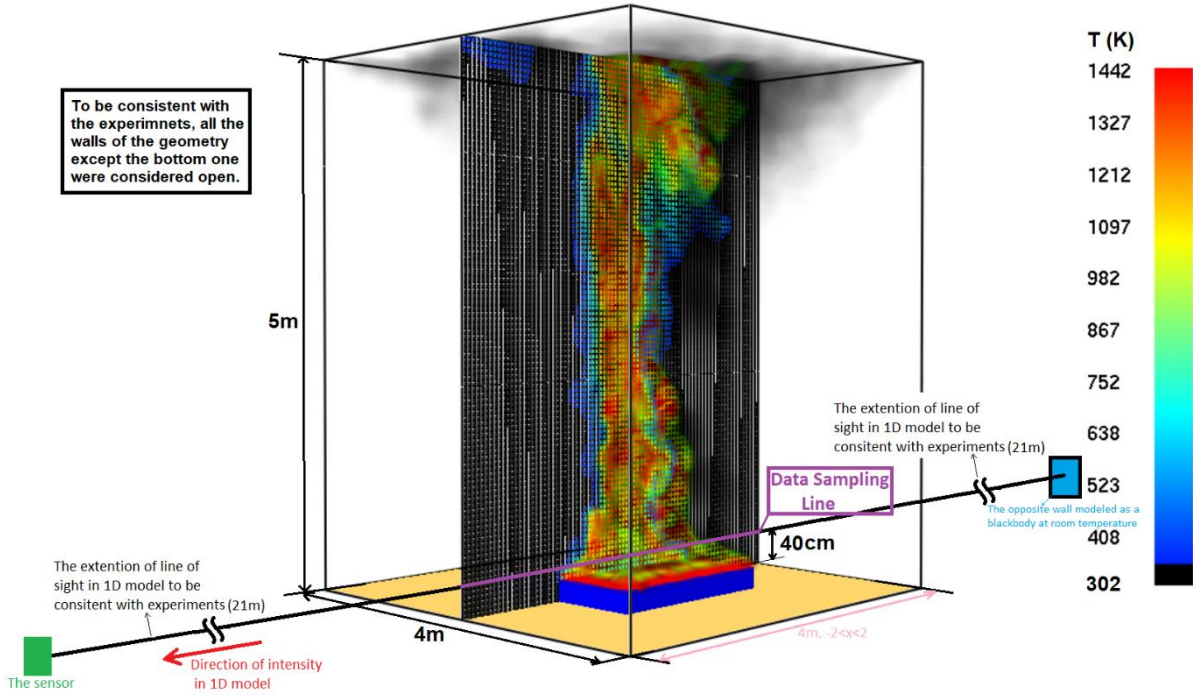

Figure 1. *An illustration of the CFD model and an instantaneous temperature profile at t=15 sec. of simulation.*

The mesh independency of the results is assured by performing one of the simulations with three different meshes of 5cm, 1cm and 0.5cm. No significant changes were observed between the two finest meshes of 1cm and 0.5 cm. However, using the CPU time of the finest grid (0.5cm) was tremendously longer than that of 1cm grid. Hence, the 1cm grid size was used to model other cases.

The transient CFD simulations were done for 20 seconds and transient profiles on the line of sight of the sensor were recorded in each 0.01 seconds resulting to 1000 sample profiles between 10 to 20 seconds in each CFD case. The first ten seconds of the simulations was not taken into account to make the simulation independent of the initial conditions. Figure 2 shows the time-averaged profiles together with standard deviation of different gas species' mole fraction, soot volume fraction and temperature along the line of sight shown in Figure 1 for two different pool sizes with a radiative fraction set to 0.3 in FDS calculations.

The time averaged experimental data of spectral radiation intensity measured at 23 meters away from the pools are used to validate the presented numerical approach.

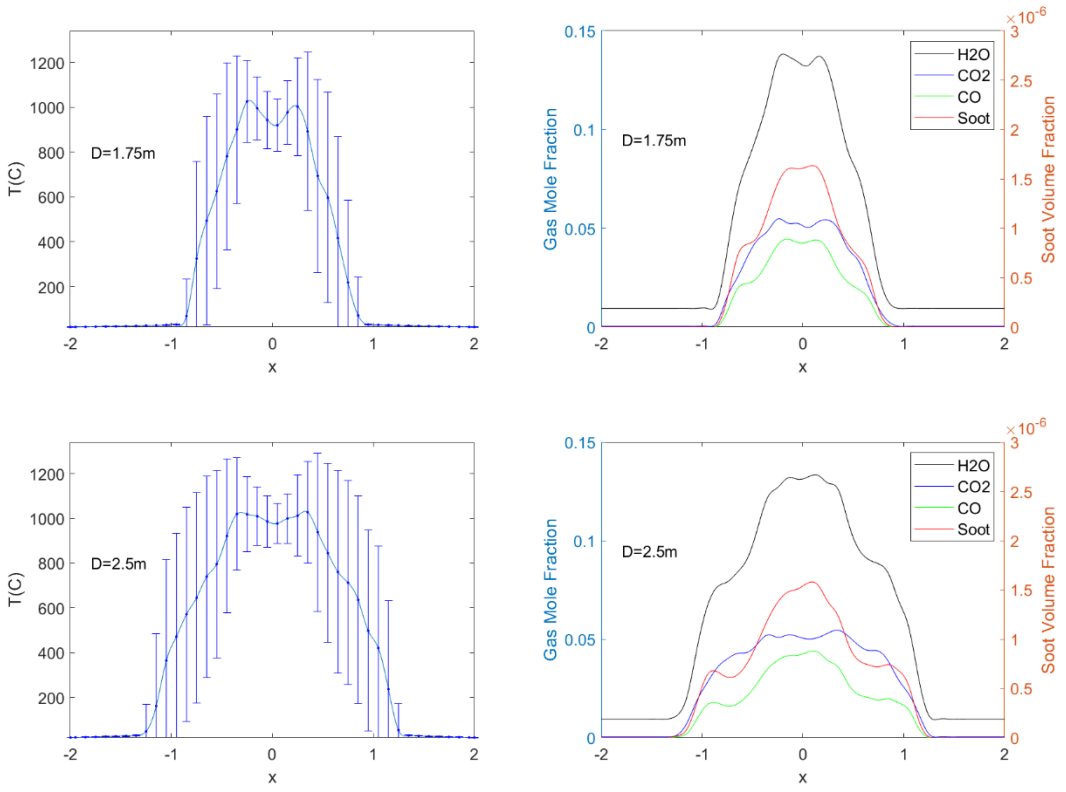

Figure 2. *Time averaged profiles along the data sampling line shown in Figure 1 with the radiative fraction set to 0.3 in CFD calculations of the 1.75 m (Top) and 2.5 m (Bottom) pools. Right: Mole fraction of gas species, and soot concentration. Left: Temperature with its standard deviation.*

1D spectral radiation model

To obtain the profile of spectral intensity reaching a sensor positioned 23 m away from the pool, a 1D model was built. According to the experimental setup a single ray solution along the sampling line is consistent with what measured in the experiments as explained in the previous sections.

The 1D models have been built for the entire line of sight starting from a point located at 23 m away from the flame on the opposite side of the sensor to the sensor, i.e. the length of the 1D models is 46m. Hence, the transient numerical profiles of each 0.01 s between 10-20 s of the simulations taken from the CFD model were extended to 23 m assuming that thermal conditions of air at the extended section are not affected by the pool fire and therefore the last data taken from the CFD model for the points on the open walls of the CFD model can be used for the rest of the line to the sensor. As an important parameter, for instance the mole fraction of water vapor on the boundary of the FDS model is calculated

as 0.0095 that corresponds to 41.5% relative humidity and it is assumed to be constant in the extended part of the 1D model which seems to be a good approximations of the typical air of the experimental space. The effect of relative humidity on the sensor's spectra is studied in the next sections. The boundary condition on the opposite wall is blackbody intensity at ambient temperature (20 °C) which is assumed to have negligible effect on the intensity spectrum reaching the sensor.

Line by line absorption spectra of combustion gases

The spectral absorption data of the gases used in the 1D model have been obtained by line-by-line calculation (LBL) with HITEMP 2010 [23].

The absorption spectra have been obtained with resolution of 0.02 cm^{-1} resulting to 492500 lines between 150-10000 cm^{-1}. The details of evaluating absorption coefficient histogram of gases as a function of wave number are described in references [12, 14]. However, to complete the current article, it is only briefly reviewed in this section.

The absorption coefficient of the optically active gases is a property which depends on the type of the molecule, wave number, temperature, partial pressure of the gas and total pressure of the gas mixture [12]. The linear absorption coefficient at an arbitrary wave number for a particular spectral line is evaluated by

$$\kappa_\eta^i = \frac{S_i}{\pi}\frac{\gamma_i}{\gamma_i^2+(\eta-\eta_i)^2} \tag{7}$$

where κ_η^i is the absorption coefficient for the ith spectral line at the η wave number location, S_i is the intensity of the ith spectral line, γ_i is the broadening of the spectral line and η_i is the spectral line location. These are the parameters which were calculated from the data given in the spectral database of HITEMP 2010 as explained below. The 0.02 cm^{-1} spectral resolution has been reported as the optimal between accuracy and CPU cost as use of higher resolutions has a negligible influence on the results but significantly increase the computational time [14]. The Lorentz profile was used for the shape of spectral lines based on the line characteristics obtained from the spectral database of HITEMP2010. For the pressures equal or higher than 1 bar and temperatures less than 2500K, the Doppler broadening is negligible and therefore Lorentz profile sufficiently describe the shape of the absorption lines [34]. A minimum limit of 10^{-9} cm^{-1} has been used for the line wings to be included (i.e. cut off limit). The intensity of each spectral Lorentz line is temperature dependent and is given as

$$S_i = S_{ref,i}\frac{Q(T_{ref})}{Q(T)}\frac{exp\left(-E_{\eta_i}/kT\right)}{exp\left(-E_{\eta_i}/kT_{ref}\right)}\frac{[1-exp(-hc\eta_i/kT)]}{[1-exp\left(-hc\eta_i/kT_{ref}\right)]} \tag{8}$$

where Q is internal partition function of the molecule at temperatures T and T_{ref}, $E_\eta$is the lower state energy of the line, k is Boltzmann constant and h is Planck constant. A reference temperature equals to 296 K was used in our LBL calculations. The collisional broadening of the spectral line depends on the temperature, partial pressure and total pressure as

$$\gamma_i = \left(\frac{T_{ref}}{T}\right)^n \left(\gamma_{air}(p_T - p_s) + \gamma_{self} p_s\right) \tag{9}$$

In order to calculate the absorption coefficient for an arbitrary wave number, the contribution of all neighboring lines needs to be considered. We simply sum up all the contributions of the spectral lines at the wave number η.

$$\kappa_\eta = \sum_i \kappa_\eta^i \tag{10}$$

The spectral line location, its intensity, air and self-broadening were taken from the spectroscopic database HITEMP 2010 [23].

Beside the combustion gases, the model used to account for soot spectral absorption coefficient in 1D model was the same as the one used in the CFD model and described in Eqs. (1-4).

RESULTS AND DISCUSSIONS

Data Sampling and Averaging

The spectra calculated by the 1D model using the instantaneous CFD profiles along the line of sight are averaged. There were 1000 samples taken from each case of the CFD model between 10-20 seconds. Running the 1D LBL calculations along the line of sight for all the samples needed tremendous CPU time and was not feasible. Hence, we selected 18 instantaneous profiles of each case for averaging. The 18 samples represent the times when the values of temperature, volume fraction of CO_2, H_2O, CO, soot and fuel are either minimum, maximum or mean in the center of the pool in the height of the line of sight. Figure 3 shows how the sensor's intensity profile calculated from this collection of 18 cases is comparable with a profile calculated from six other randomly selected samples and with the combination of 18 and 6 cases. The difference between the profiles resulting from 18 and 24 samples is negligible. Hence, one can conclude that the profile obtained by 18 or 24 samples adequately represents the time averaged profile of the flame reaching the sensor.

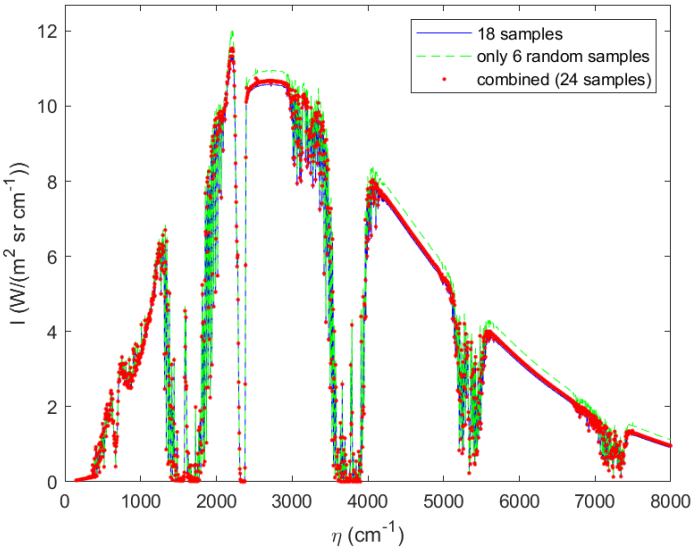

Figure 3. *Comparison of smoothed intensity profiles calculated by averaging 18 strategically selected transient CFD profiles samples, 6 other random samples and a combination of these two, i.e. 24 samples. The data are from the 2.5 m pool with radiative fraction set to 0.3.*

The spectral resolution of the numerical data was 0.02 cm^{-1} which is much higher than that of experiments (4 cm^{-1}). Hence, the numerical results were smoothed to provide a better ground for comparison and validation. The smoothed and unsmoothed averaged numerical intensity profiles reaching the sensor from the 2.5 m pool with the radiative fraction of 0.3 are shown in Figure 4.

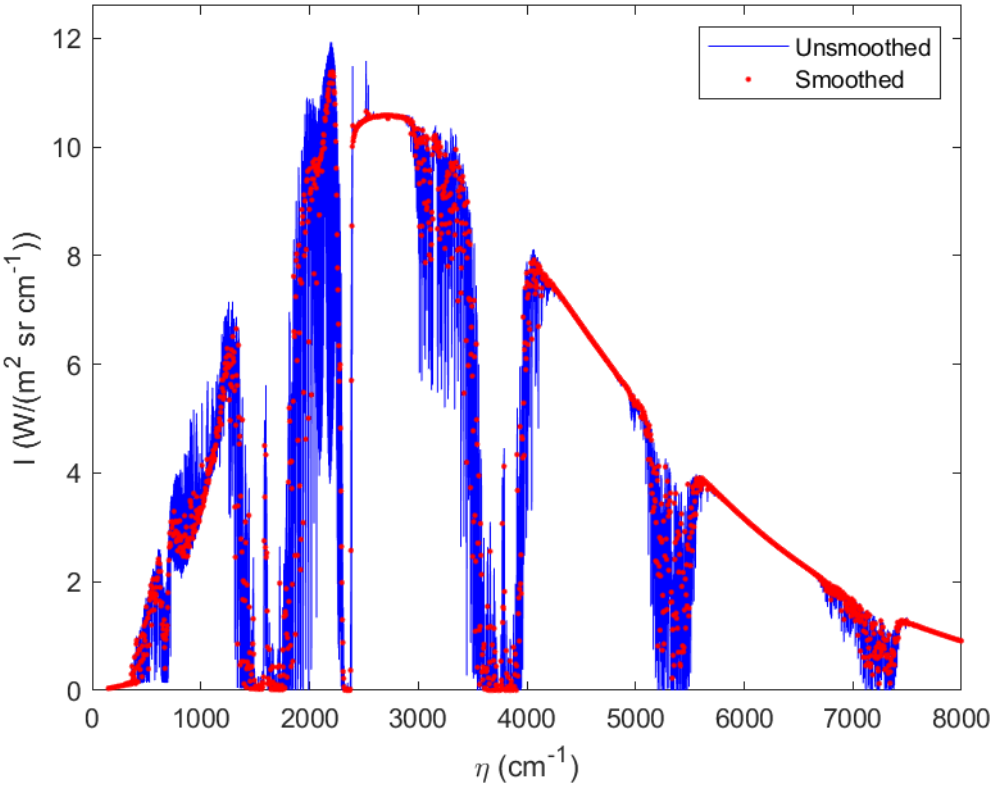

Figure 4. *The smoothed and unsmoothed averaged numerical intensity profiles reaching the sensor from the 2.5m pool with the radiative fraction of 0.3*

Numerical vs Experimental Results and the Effect of the Radiative Fraction

The smoothed numerical intensity profiles of both cases (D=1.75 m and D=2.5 m) are compared with their experimental counterpart in Figure 5. This figure shows the numerically calculated smoothed radiation intensity reaching the sensor compared with the experimental ones together with Planck intensity profiles of two relevant temperatures. As explained before, the specified radiative fraction in FDS compensates the inaccuracy of the flame zone emission term, caused by using relatively coarse computational grid in engineering models of fires and by lack of explicit model for the turbulence-radiation interaction. For the Kerosene pool fires studied in this research, the radiative fraction is experimentally reported to be 0.3 [31]. Figure 5 shows that although both modeling options $\chi_r = 0$ and $\chi_r = 0.3$ in the CFD model could fairly predict the experimental profiles, neither of them provides accurate prediction over the entire spectrum. While introducing $\chi_r = 0.3$ to the model makes the peak of the profile (~2000-3000 cm^{-1}) closer to the experimental data, it causes over prediction in larger wavenumber (>4000cm^{-1}) which corresponds to emission of hotter zones of the flame.

Comparing the numerical and experimental profiles with the two blackbody profiles shows that neither of

the blackbody profiles, which are representative of soot radiation at these temperatures, match well with the non-absorbed parts of the spectral intensity profiles over the entire spectrum. At large wavenumbers (>4000 cm^{-1}), the blackbody profile of 1250 K agrees well with the non-absorbed parts of the spectrum. However, for the small wavenumbers (<1000 cm^{-1}), the 1100 K blackbody profile more accurately represents the observed flame intensity profile. This behavior is explained by the contributions of soot emissions from the different temperatures along the line of sight of the sensor. This result indicates the need for a better approximation than single flame temperature in estimating the flame emission in engineering calculations.

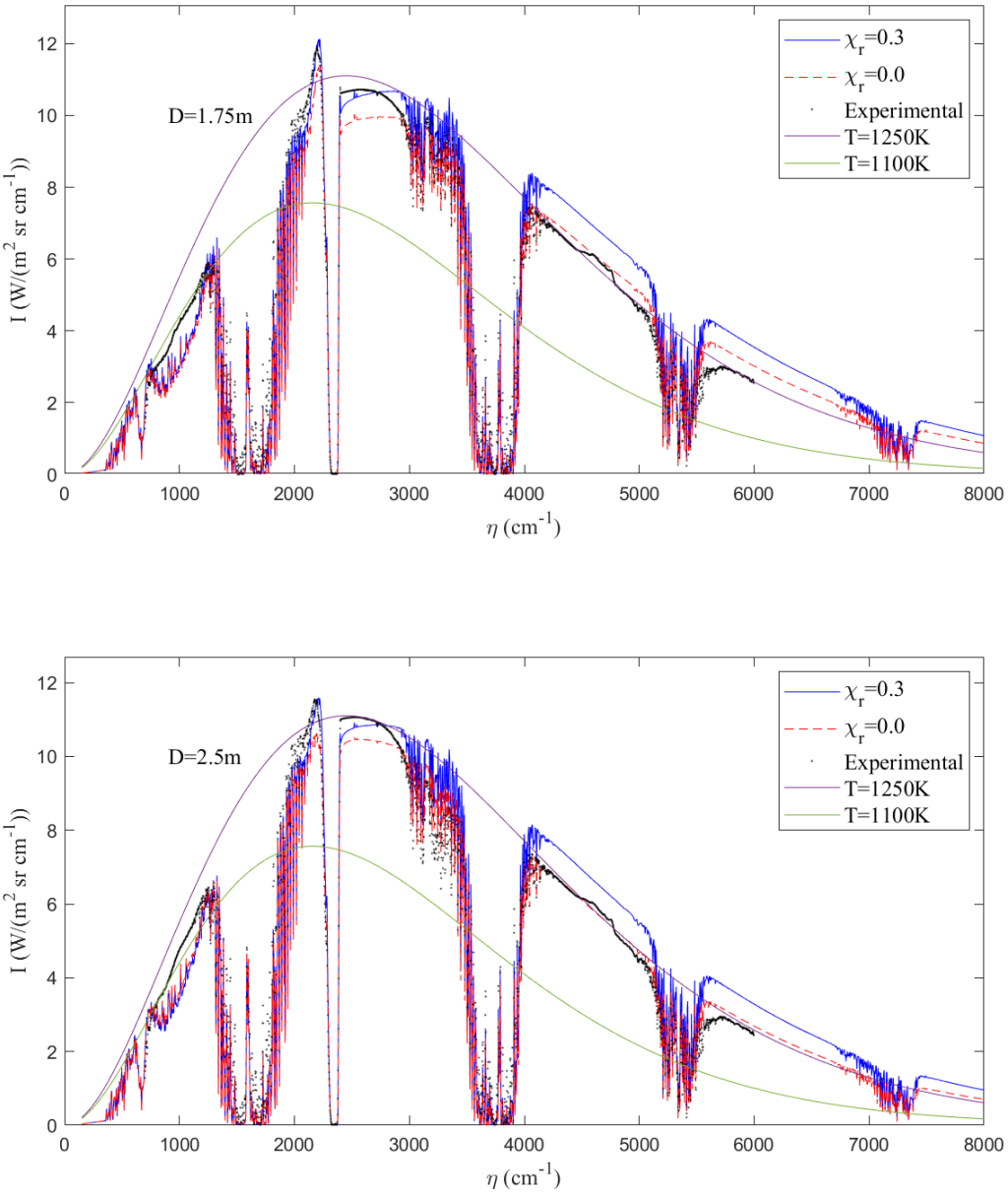

Figure 5: *Smoothed numerical and experimental intensity profiles of D=1.75 m and D=2.5 m pools, calculated from the CFD data with specified and un-specified radiative fractions, compared to blackbody intensity profiles of two temperatures.*

Figure 5 also shows the strong absorption effect of atmospheric cold gases, which explains the peak and valley-like regions in both numerical and experimental spectra. Figure 6 exhibits how the band center and width of the absorption bands of gases are changing with temperature. It shows the location of main absorption bands of H_2O, CO_2 and CO are slightly shifted with temperature. In addition, the width of the

bands is also affected by temperature. The effect of this changes with temperature is seen in the radiation spectrum of the flame shown in Figures 4 and 5. The absorption spectra of CO_2 at 300K and 1250K which is around the maximum temperature of our 1D model are seen in Figure 6. While the cold atmospheric CO_2 causes the strong absorption from the flame at wavenumbers around 2300-2380 cm^{-1}, the strong emission of hot CO_2 within the flame occurs at lower wavenumbers. Hence, the emission from hot gases can be transferred through the transparent window of the cold CO_2 while the strong absorption of cold atmospheric CO_2 blocks the flame radiation at larger wavenumber (~2250-2400 cm^{-1}) corresponded to emission from soot. However, in both spectra, an emission peak of hot CO_2 gases at ~2200 cm^{-1} is clearly distinguishable even at 23 meters away from the flame. This can be used for detecting fires from other hot resources by optical fire detection sensors. Development of fire detection paradigm based on this spectral feature is a part of our ongoing research.

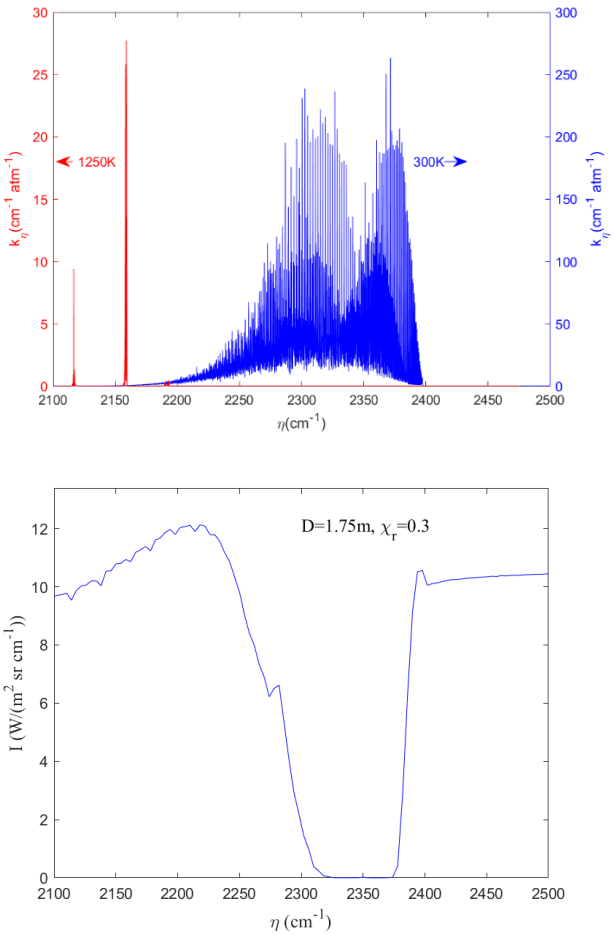

Figure 6: *Top: sample of changes of spectral characteristics of the absorption band of CO_2 with temperature. Bottom: The peak and valley-like part of the intensity spectra caused by change of characteristics of hot and cold CO_2around 2100-2400 cm^{-1}.*

Effect of pool size

Figure 7 compares the numerical radiative intensity profiles of two pool sizes. As expected, the intensity

coming from the larger pool is stronger. Most of the absorption regions are identical which is because of the strong absorption effect of atmospheric gases between the pool and the sensor. Moreover, the emission peak of hot CO_2 is more distinguishable in the smaller pool which is explained by the larger optical thickness of the larger pool which makes the flame emissivity closer to one for most of the spectrum. Hence, one can expect that higher optical path of soot emission in the larger pool makes the radiative intensity profile leaving the flame zone closer to that of a hot blackbody. Therefore, detecting optically thicker fires through their spectral characteristics is more challenging as they are difficult to distinguish from other hot objects. Nonetheless, the optical fire detection aims at detecting fires quickly before they become large.

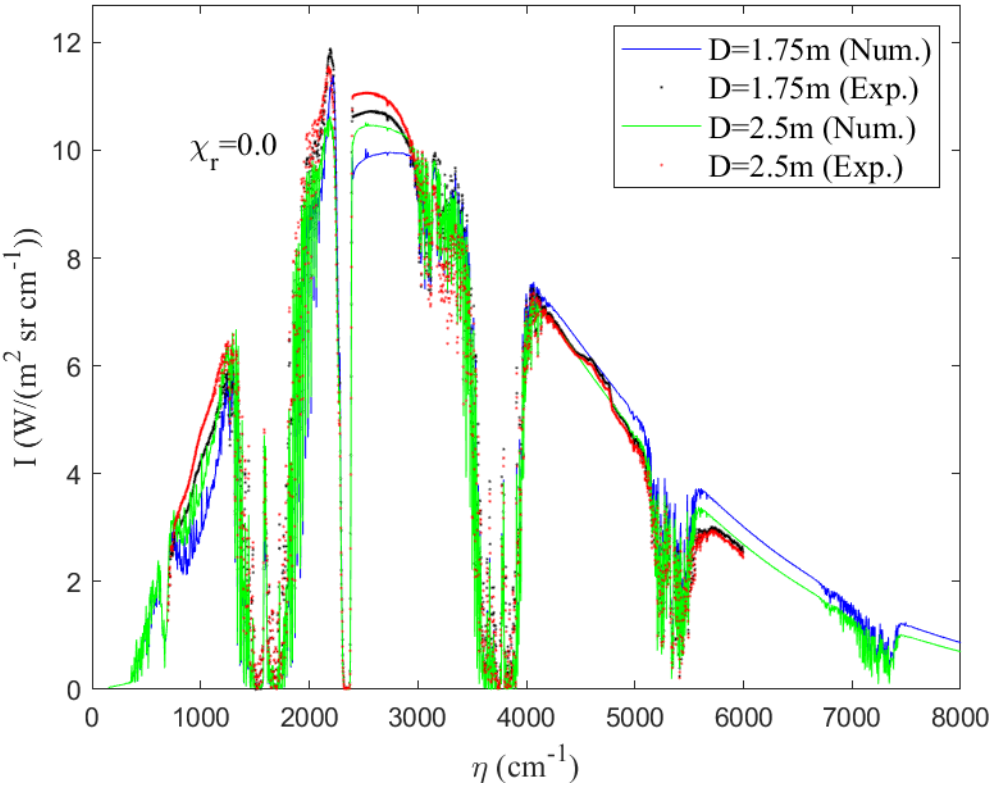

Figure 7. *Effect of the pool size on the predicted and measured intensities.*

Comparison with a Blackbody Emitter

To identify the main spectral characteristics of the fire radiation intensity spectrum that make it distinguishable from a hot object, the 1D model is adopted. A blackbody with the similar temperature as the maximum temperature of fire profiles, i.e. 1250 K, is placed as the source of radiation at one end of the 1D model (i.e. 23m). The participating media is assumed to be air with 0.95% (RH=41.5%) of H_2O and 0.04 % of CO_2 at room temperature (20 °C).

Figure 8 shows the observed radiation spectra from a 2.5 Kerosene pool fire and from the hot blackbody source. The Planck intensity profile at the same temperature (1250K) is also included in the figure for comparison. The emission peak of CO_2 is seen as the characteristic feature of the fire spectrum compared to the spectrum of a hot blackbody. Moreover, in case of blackbody source, the Planck distribution can successfully describe the non-absorbed parts of the entire spectrum. In contrary, for the fire spectrum, a single Planck distribution cannot represent the intensity in all spectral regions because the profile of fire is contributed by soot emission from different temperatures, as explained before and shown in Figure 5. Nonetheless, experimental observations [20] show that the non-gray behavior of soot is expected to be more important in flame intensity of smaller fires. In large pools, the large optical thickness of the flame makes the flame emissivity close to one for most of the wavelengths, but it does not occur in smaller flames with smaller optical thicknesses.

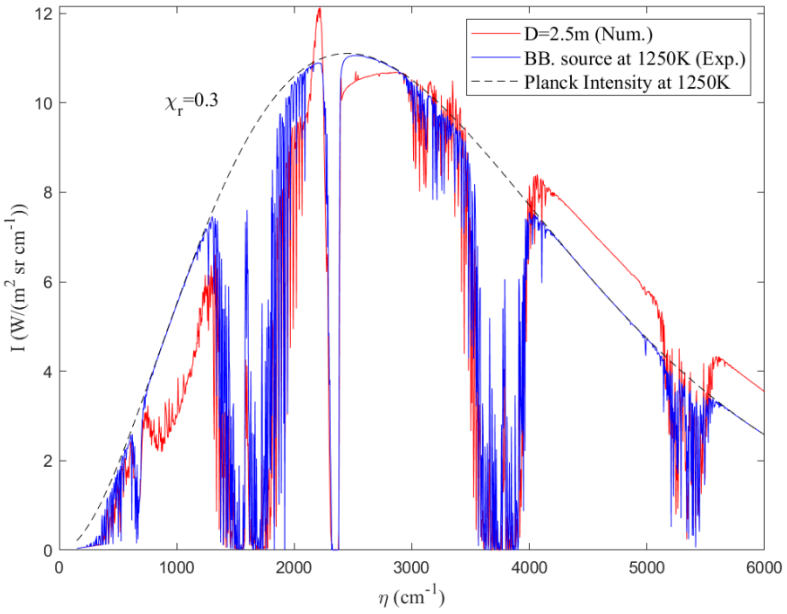

Figure 8. *Spectrum coming from a hot blackbody at T=1250K compared with the one coming from a fire flame of 2.5m pool and Planck intensity profile of 1250K.*

Effect of Relative Humidity

To study the effect of the air relative humidity on the intensity spectrum reaching the sensor, the 1D LBL calculations of 2.5 m pool with radiative fraction of 0.3 are repeated in a condition with 100 % relative humidity. This corresponds, for instance, to the conditions when sprinklers are activated in a fire compartment.

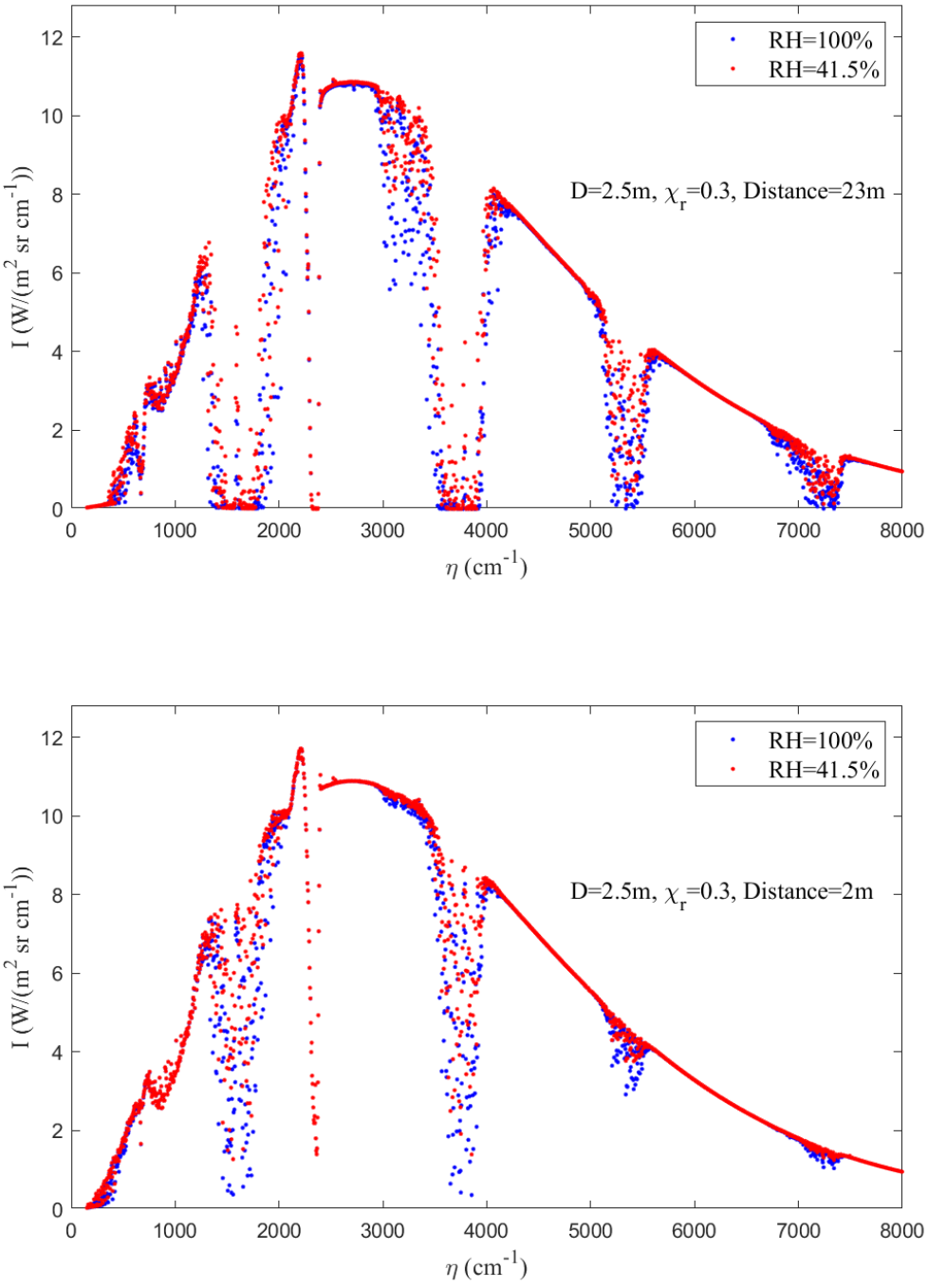

Figure 9. *Intensity reaching the sensor at two different distances from the pool in two different relative humidity of 41.5% and 100%.*

Figure 9 compares the intensity spectra recorded at 2 m and 23 m distances from the center of the pool. At the 23 m distance, the difference between the two humidity levels is negligible in most parts of the spectra. A slightly larger absorption effect can be seen for the RH=100% in parts of the spectrum corresponding to the main absorption bands of H_2O. At 2 m distance, the difference is more remarkable. For instance, we clearly see that the higher moisture content causes absorption valleys and deviations from the blackbody profile.

Effect of the Sensor Distance

While the intensity profile near or inside the flame are difficult to measure experimentally, the developed numerical model can provide adequate insight on how the intensity spectrum of a pool fire is changing along the line of sight of a sensor. Figure 10 shows the intensity spectra at different distances from the center of the pools. As seen, within the flame the emission of hot gases and soot are quite dominant. However, gradually the effect of cold atmospheric gases decreases the intensity in different spectral regions corresponded to the main absorption bands of CO_2 and H_2O while the rest of the spectrum, corresponding to the emission of soot, remains unchanged.

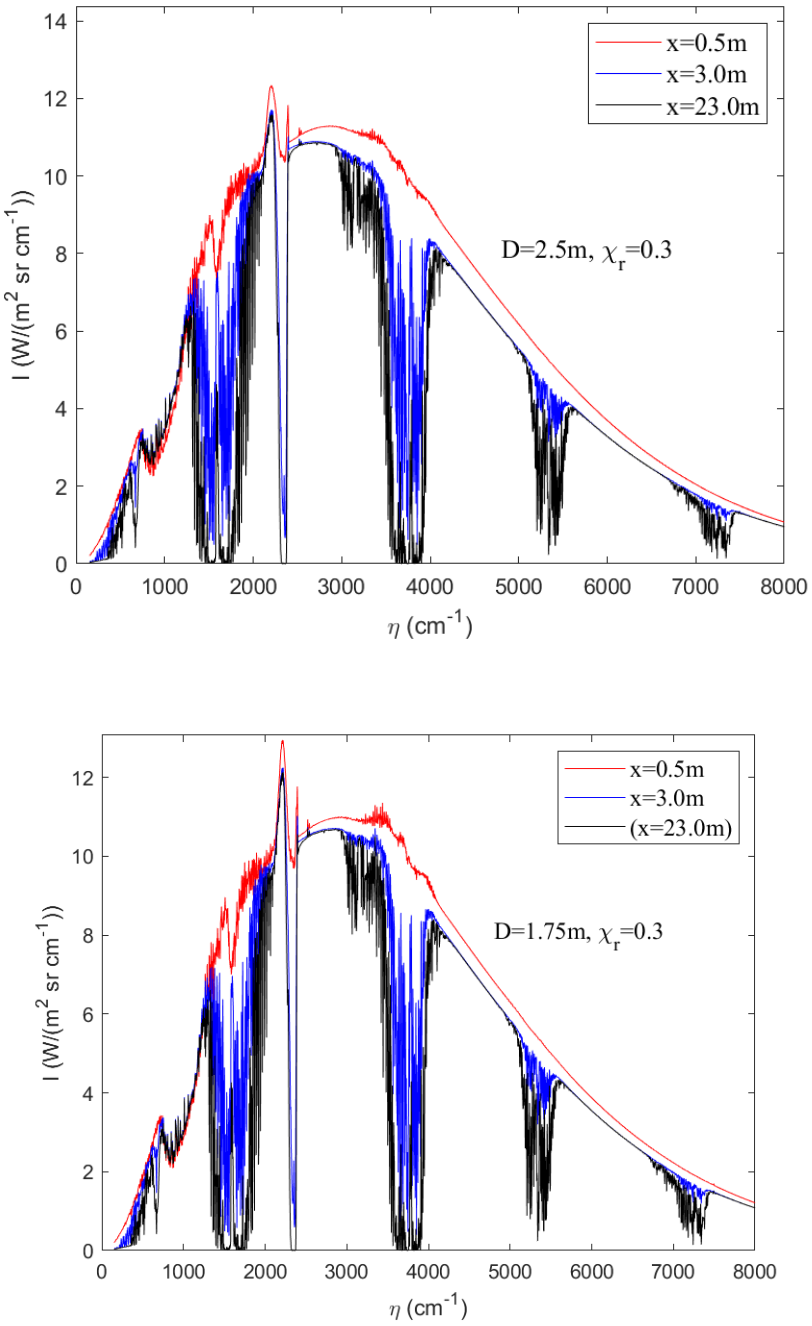

Figure 10. *Change of the intensity profile along line of sight at different distances from the center of the pools.*

CONCLUSIONS

The spectral radiation of large Kerosene pool fires was numerically computed. The numerical approach was based on collecting transient data of temperature, gas species and soot profiles as samples of instantaneous profiles from 3D CFD models of 1.75 m and 2.5 m Kerosene pool fires, and using them in a 1D solution of spectral radiation along a line of sight of a sensor located outside the flame zone. The spectral absorption of combustion gases was obtained through the line-by-line calculations using the HITEMP 2010 spectral database. The intensity predictions corresponding to the instantaneous CFD profiles were averaged and compared to the experimentally measured intensity spectra of the same setup.

While the absorption effect of cold atmospheric gases is quite noticeable in spectral locations of absorption dominant parts of flame spectra, an emission peak of hot CO_2 at ~2200 cm^{-1} has been consistently found in all the simulations which was in-line with the reported experimental observations. The large absorption regions due to the cold, strongly absorbing atmospheric gases such as CO_2 and H_2O formed valley-like spectral regions in the intensity profiles reaching the sensors. The effect of temperature in shifting the center location and size of the CO_2 absorption band causes a strong horn like region in the spectra. Compared to the spectra obtained for the hot blackbody, this emission peak can be therefore identified as the characteristic feature of fire flames and used for designing spectral based fire detection systems.

The results proved that a single Planck distribution cannot fully describe the non-absorbed parts of the spectrum observable outside the flame region. The continuous parts of the spectra were found to consist of contributions of soot emission taking place at various temperatures along the line of sight. More work is needed to develop an engineering model that effectively captures this phenomenon in a simple yet accurate way.

A sensitivity analysis was performed to investigate the effects of the pool size, distance from the pool, and the air relative humidity. The results showed that inside the flame, the emission dominates the radiation spectra, but as the distance from the pool increases, the absorption of cold atmospheric gases drastically changes the shape of the spectra causing valley-like absorption regions. Increasing relative humidity expectedly amplifies the water-related absorption regions of the spectrum but has no effect on the other parts of the spectra.

As expected, the spectrum coming from a larger pool was stronger than that of the smaller pool. Also, it was closer the spectrum from a hot black body. It is in turn attributed from that the larger optical thickness of the larger pools. Due to the smaller optical thickness of the smaller pools, the differences of their spectra with those of hot blackbody objects are larger and therefore their spectra would be easier to be detected. For the smaller pools, the CO_2 emission peak is more clearly distinguishable, which is due to the smaller optical thickness of smaller pool fires. In larger pool fires, the large optical thickness

makes the flame emissivity close to one in most of the spectrum and therefore the flame spectra behave in a more blackbody like manner.

As next step, this research is currently continued with FDS modeling of smaller pools and more quantitative validation against new experimental data measured for smaller n-heptane and Kerosene pool fires. Averaging all the instantaneous profiles which need a few months of computations is a part of our ongoing research. More importantly, the current modeling framework and the available experimental data pave a road to address the effects of the different empirical aspects in the radiation modelling of large fires.

ACKNOWLEDGEMENT

This work has been funded by the Academy of Finland under Grant No 314487.

REFERENCES

[1] M. H. Bordbar and T. Hyppänen, "Multiscale numerical simulation of radiation heat transfer in participating media," *Heat Transfer Engineering,* vol. 34, pp. 54-69, 2013.

[2] B. Wu, S. P. Roy, X. Zhao and M. F. Modest, "Effect of multiphase radiation on coal combustion in a pulverized coal jet flame," *Journal of Quantitative Spectroscopy and Radiative Transfer,* vol. 197, pp. 154-165, 2017.

[3] M. H. Bordbar and P. Zamankhan, "Dynamical states of bubbling in vertically vibrated granular materials. Part I: Collective processes," *Communications in Nonlinear Science and Numerical Simulation,* vol. 12, pp. 254-272, 2007.

[4] M. H. Bordbar and P. Zamankhan, "Dynamical states of bubbling in vertical vibrated granular materials. Part II: Theoretical analysis and simulations," *Communications in Nonlinear Science and Numerical Simulation,* vol. 12, pp. 273-299, 2007.

[5] M. H. Bordbar and T. Hyppänen, "SIMULATION OF BUBBLE FORMATION AND HEAPING IN A VIBRATING GRANULAR BED," *Chemical Engineering Communications,* vol. 198, no. 7, pp. 905-919, 2011.

[6] M. Darbandi and B. Abrar, "Thermal radiation transfer calculations in combustion fields using the SLW model coupled with a modified reference approach," *Journal of Quantitative Spectroscopy and Radiative Transfer,* vol. 205, pp. 105-113, 2018.

[7] F. Alinejad, H. Bordbar and S. Hostikka, "Development of full spectrum correlated k-model for spectral radiation penetration," *International Journal of Heat and Mass Transfer,* p. in press, 2020.

[8] I. Sikic, S. Dembele and J. Wen, "Non-grey radiative heat transfer modelling in LES-CFD simulated methanol pool fires," *Journal of Quantitative Spectroscopy and Radiative Transfer,* vol. 234, pp. 78-89, 2019.

[9] F. Liu, G. J. Smallwood and W. Kong, "The importance of thermal radiation transfer in laminar diffusion flames at normal and microgravity," *Journal of Quantitative Spectroscopy and Radiative Transfer,* vol. 112, pp. 1241-1249, 2011.

[10] H. bordbar and S. Hostikka, "Numerical Solution of LBL Spectral Radiation of a Heptane Pool Fire," in *The proceeding of the 9th International Symposium on Radiative Transfer, RAD-19*, Athens, Greece, 2019.

[11] H. Chu, J.-L. Consalvi, M. Gu and F. Liu, "Calculations of radiative heat transfer in an axisymmetric jet diffusion flame at elevated pressures using different gas radiation models," *Journal of Quantitative Spectroscopy and Radiative Transfer,* vol. 197, pp. 12-25, 2017.

[12] M. H. Bordbar, G. Wecel and T. Hyppänen, "A line by line based weighted sum of gray gases model for inhomogeneous CO2–H2O mixture in oxy-fired combustion," *Combustion and Flame,* vol. 161, no. 9, p. 2435–2445, 2014.

[13] C. Wang, B. He, M. F. Modest and T. Ren, "Efficient full-spectrum correlated-k-distribution look-up table," *Journal of Quantitative Spectroscopy and Radiative Transfer,* vol. 219, pp. 108-116, 2018.

[14] H. Bordbar and T. Hyppänen, "Line by line based band identification for non-gray gas modeling with a banded approach," *International Journal of Heat and Mass Transfer,* vol. 127, pp. 870-884, 2018.

[15] H. Bordbar, A. Maximov and T. Hyppänen, "Improved banded method for spectral thermal radiation in participating media with spectrally dependent wall emittance," *Applied Energy,* vol. 235, pp. 1090--1105, 2019.

[16] H. Bordbar, G. Fraga and S. Hostikka, "An Extended Weighted-Sum-of-Gray-Gases Model to Account for All CO2-H2O Molar Fraction Ratios in Thermal Radiation," *Intenrnational Communications in Heat and Mass Transfer,* p. In press, 2019.

[17] H. Chu, F. Liu and H. Zhou, "Calculations of gas thermal radiation transfer in one-dimensional planar enclosure using LBL and SNB models," *International Journal of Heat and mass transfer,* vol. 54, p. 4736–4745., 2011.

[18] G. Fraga, H. Bordbar, S. Hostikka and F. H. R. Franc¸a, "High-Fidelity Numerical Data for Non-Gray Radiative Transfer in Three-Dimensional Benchmarks Using Line-by-Line Integration," *Journal of Heat Transfer-T ASME,* p. in press, 2019.

[19] J. M. Suo-Anttila, T. K. Blanchat, A. J. Ricks and A. L. Brown, "Characterization of thermal radiation spectra in 2m pool fires," *Proc. Combust. Inst.,* vol. 32, pp. 2567-2574, 2009.

[20] G. Parent, G. Erez, A. Collin, M. Suzanne, A. Thiry-Muller, M. Weber, E. Faure and P. Boulet, "Spectral radiation emitted by kerosene pool fires," *Fire Safety Journal,* vol. 108, p. 102847, 2019.

[21] H. Bordbar and S. Hostikka, "NUMERICAL SOLUTION OF LBL SPECTRAL RADIATION OF A N-HEPTANE POOL FIRE," in *The 9th International Symposium on Radiative Transfer, RAD-19*, Athens, Greece, 2019.

[22] K. McGrattan, R. McDermott, J. Floyd, S. Hostikka, G. Forney and H. Baum, "Computational fluid dynamics modelling of fire," *International Journal of Computational Fluid Dynamics,* vol. 26, pp. 349-361, 2012.

[23] L. S. Rothman, I. E. Gordon, R. J. Barber, H. Dothe, R. R. Gamache, A. Goldman, V. I. Perevalov, S. A. Tashkun and J. Tennyson, "HITEMP, the high-temperature molecular spectroscopic database," *Journal of Quantitative Spectroscopy and Radiative Transfer,* vol. 111, pp. 2139-2150, 2010.

[24] G. Erez, G. Parent, A. Collin, P. Boulet, M. Suzanne, E. Faure and A. Thiry-Muller, "Flame properties of large kerosene fires," *Journal of Physics: Conference Series,* vol. 1107, p. 042035, 11 2018.

[25] K. McGrattan, S. Hostikka, R. McDermott, J. Floyd, C. Weinschenk and K. Overholt, "Fire Dynamics Simulator; User's Guide," National Institute of Standards and Technology, Gaithersburg, Maryland, USA, 2013.

[26] V. R. Lecoustre, "RadCal; Improvements to the Narrow-Band Model for Radiation Calculations in a combustion Environment," NIST Special Publication 1402, Second Edition, 2014.

[27] H.-c. Chang and T. T. Charalampopoulos, "Determination of the wavelength dependence of refractive indices of flame soot," *Proceedings of the Royal Society of London. Series A: Mathematical and Physical Sciences,* vol. 430, pp. 577-591, 1990.

[28] M. F. Modest, "Chapter 12 - Radiative Properties of Particulate Media," in *Radiative Heat Transfer (Third Edition)*, Third Edition ed., M. F. Modest, Ed., Boston, Academic Press, 2013, pp. 387-439.

[29] G. D. Raithby and E. H. Chui, "A Finite-Volume Method for Predicting a Radiant Heat Transfer in Enclosures With Participating Media," *Journal of Heat Transfer,* vol. 112, pp. 415-423, 5 1990.

[30] K. McGrattan, S. Hostikka, R. McDermott, J. Floyd and M. Vanella, "Fire Dynamics Simulator; Technical Reference Guide, Volume 1: Mathematical Model,," National Institute of Standards and Technology, Gaithersburg, Maryland, USA, 2019.

[31] K. B. McGrattan, H. R. Baum and A. Hamins, "Thermal Radiation from Large Pool Fires," National Institute of Standards and Technology, Gaithersburg, Maryland, USA, 2000.

[32] D. D. Drysdale, Introduction to fire Dynamics, 3rd ed., John Wiley and Sons, 2011, 2011.

[33] E. W. Lemmon and M. L. Huber, "Thermodynamic Properties of n-Dodecane," *Energy & Fuels,* vol. 18, pp. 960-967, 2004.

[34] A. Wang and M. F. Modest, "Importance of Combined Lorentz-Doppler Broadening in High-Temperature Radiative Heat Transfer Applications," *Journal of Heat Transfer,* vol. 126, pp. 858-861, 11 2004.

[35] F. Liu, C. Wong, D. R. Snelling and G. J. Smallwood, "Investigation of Absorption and Scattering Properties of Soot Aggregates of Different Fractal Dimension at 532 nm Using RDG and GMM," *Aerosol Science and Technology,* vol. 47, pp. 1393-1405, 2013.